Sensors & Actuators: B. Chemical 336 (2021) 129656

Stretchable electrical cell-substrate impedance sensor platform for monitoring cell monolayers under strain

Chen Zhou a, 1, Sebastian Bette a, 1, Aaron Babendreyer b, Christina Hoffmann c, Sven Gerlach c, Tom Kremers a, Andreas Ludwig b, Bernd Hoffmann c, Rudolf Merkel c, Stefan Uhlig b, d,

Uwe Schnakenberg a,*

a Institute of Materials in Electrical Engineering 1 (IWE1), RWTH Aachen University, Sommerfeldstrasse 24, 52074, Aachen, Germany

b Institute of Molecular Pharmacology, RWTH Aachen University, Wendlingweg 2, 52074, Aachen, Germany

c Institute of Biological Information Processing (IBI-2): Mechanobiology, Forschungszentrum Jülich GmbH, Leo-Brandt-Strasse, 52425, Jülich, Germany

d Institute of Pharmacology and Toxicology, RWTH Aachen University, Wendlingweg 2, 52074, Aachen, Germany

A R T I C L E I N F O

Keywords:

ECIS

Microelectrodes PDMS

Mechanosensation A549

MDCK

A B S T R A C T

Stretchable microelectrodes paired with an ultra-elastic substrate can be used for electrical sensing of mechanically stretched cells and cell monolayers. Here, we present the development of a cell-stretching platform with thin-film interdigitated microelectrodes. Up to 35 % cyclic stretch are feasible with a novel interlaced meander design connected to the microelectrodes and using Poly(dimethylsiloXane) (PDMS) with a Young's modulus of 50 kPa as an ultra-elastic substrate. Reliable electrical contacting of the microelectrodes under stretch was achieved by perforation of the contact pads. The novel platform enables label-free, real-time electrical cellsubstrate impedance (ECIS) monitoring of cell monolayers. Proof-of-concept experiments indicated that electrical impedance of Madin-Darby canine kidney (MDCK) cell monolayers increased sharply by uniaxial mechanical strain above 20 %. For comparison, human alveolar basal epithelial adenocarcinoma (A549) cell monolayers, which are known to lack mature cell junctions, showed a continuous decrease of electrical impedance over the whole applied strain range of 35 %. The data reveal that impedance changes upon stretching depend on epithelial cell types and existence of tight cellular junctions. The system provides the basis for reliable continuous long-term monitoring of electrical properties of cell monolayers under strain by electrical impedance spectroscopy, e.g., to monitor epithelial permeability changes in real time and under label-free conditions to screen the influence of pharmacological substances.

1. Introduction

The integration of electronics with flexible as well as stretchable materials has led to a remarkable increase of new technological developments and applications [1–5]. In particular, the interaction of flexible and stretchable devices with biological tissues is gaining special attention for applications such as brain interface [6,7], epidermal sensing [8–10], or cardiac electrotherapy [11]. Furthermore, studies of fundamental processes in mechanobiology are gaining increasing interest and importance through the use of stretchable devices. Mechanobiology deals with the influence of mechanical signals on development, differentiation, physiology, and metabolism of single cells, cell monolayers, and tissues [12,13]. There is a tremendous

interest in developing methods to apply well-defined mechanical stimuli in physiologically relevant ranges [14]. The stretching of cells, cell layers and tissues is one of the most fundamental stimuli. Both, uniaxial as well as biaxial setups are in use. Uniaxial stretchers allow cells to be stretched in one direction while experiencing compression in the perpendicular direction. The effect of shear stress can be minimized by the system and membrane design. Biaxial stretchers allow the cells to be stretched along two axes perpendicular to each other without shear stress [15]. In both setup types elastic membranes are utilized, typically made of Poly(dimethylsiloXane) (PDMS), with tunable stiffness coated with a cell matriX protein on which cells are grown. PDMS is biocompatible, exhibits low autofluorescence and is transparent. It is worthwhile to note that PDMS is stretchable to physiologically relevant ranges

* Corresponding author.

E-mail address: schnakenberg@iwe1.rwth-aachen.de (U. Schnakenberg).

1 These authors contributed equally to the work.

https://doi.org/10.1016/j.snb.2021.129656

Received 13 October 2020; Received in revised form 29 January 2021; Accepted 8 February 2021

Available online 13 February 2021

with an approximately linear material behavior [16].

In uniaxial stretch setups, a rectangular membrane is clamped at two opposite sides while the other two sides are left free. The membrane can be stretched by using stepper motors [15,17,18], cams [19–22], magnets [23,24], a vacuum [25], indenters [26], or piezoelectric actuators [27]. In devices using cams, the cam has to be exchanged for different stretching protocols. The piezoelectric actuator allows for precise stretching in the range of several tens of micrometers. In one approach, sophisticated MEMS (micro-electro-mechanical systems) techniques with micromolding and multiple exposure of SU-8 photoresist were developed to fabricate a microlinkage mechanism for uniaxial stretch [28,29]. Commercially available uniaxial stretching devices, like NS-300 (Strex Inc., Osaka, Japan), were also used [30].

Biaxial stretcher setups, which apply pressure or vacuum to one side of a circularly clamped membrane cause an inflation and hence a stretching in radial as well as circumferential directions [31–34], were developed. It is worthwhile to note that equibiaxial and uniform strain in this type of setup is only localized in the center of the membrane [35]. For equibiaxial membrane stretching, commercially available systems of FlexCell International (Hilbsborough, NC, USA) are used to apply strain to the membrane by drawing it over a circular loading post and applying vacuum [16,36,37]. Custom-made setups using the same principle were developed [38]. Colombo et al. carefully calibrated pressure-strain curves [37]. In this respect, mechanical actuated setups with motors seem to perform better than vacuum-actuated devices due to a precise adjustment of the strain [24]. In-plane membrane stretching

is also possible when the membrane is pressed close to a thin glass bottom slide and extends in the x–y plane by applying vacuum [39]. In this approach, uniaxial as well as equibiaxial stretching depends on the design of the vacuum chamber.

An interesting iris-type expansion device was developed by Majd et al. in which several micromotors were connected to the rim of a circularly-shaped membrane [40]. By actuation, the motors expand the membrane equibiaxially. Furthermore, equibiaxial as well as uniform membrane stretching can be carried out by utilizing an indenter to indend the circular membrane dynamically [41], often with the use of a cam [35,42,43].

For setups that are working with in-plane membrane stretching, the strain is uniform in the central area of the membrane [35,43], which can be verified by tracking of fluorescent particles in the membrane [18,44], posts [37,45], markers [35,43] as well as fluorescent-labeled molecules or spheres micropatterned on the membrane [16,19,25,39,41,46].

Setups working with in-plane membrane stretching enable light microscopic real-time life-cell imaging at high resolution which is not possible with membrane inflation and indenter approaches.

To summarize, a precisely defined uniaxial strain can easily be generated by stretching an elastic membrane via a linear translation

of cells and cell layers subjected to an electric field [51]. Advantageously, thin-film electrodes can easily be deposited on planar substrates. By applying AC voltages across the immobilized cell or cell layer, the corresponding current is measured. Using epithelial or endothelial cell layers, the transepithelial or transendothelial impedance (TER) is calculated. A recently published review paper by Le et al. [52] cited that the data obtained can, inter alia, be related to morphological changes of the cell layer, such as cell spreading [53], shape changes [54], adhesion [55], migration and micro-motion [50,56], adherence, differentiation [57], proliferation, barrier function, and motility [58] with high sensitivity and temporal resolution. The advantage of ECIS is the use of microelectrode arrays to determine TER at different positions of the cell layer and to carry out impedance sensing under normal culture conditions [53].

The focus of the present work is on the development of a novel

versatile cell-stretching platform that enables ECIS measurements under stretching conditions. In our previous work, highly stretchable meandertype structures have already been reliably fabricated on the bottom of a well-characterized stretchable cell culture chamber made of PDMS with a Young's modulus of only 50 kPa that permits superior stretchability [59]. To mimic the mechanical environment of cell layers in-vitro, substrates of physiological relevant stiffness in the kPa-range must be used. In this work, interdigitated microelectrodes and interlaced meanders are favorably combined for the first time for a stretchable ECIS sensor on very soft substrates. Compared to electrodes located far away, interdigitated microelectrodes are surface and therefore cell layer sensitive by confining the electric field close to the sensor surface while reducing the spreading of electrical field lines into the bulk [60,61].

Furthermore, this work extends the idea of stretchable interconnects to interdigitated microelectrodes on stretchable PDMS. A novel method of micro-welding gold wires for connecting stretchable electrodes is also demonstrated, enabling reliable communication even during long-term cyclic stretching experiments.

As proof-of-concept, first experiments were carried out by real-time ECIS monitoring of two types of cell monolayers under strain, one with and one without forming mature cell junctions, showing the capability of performance of the ECIS sensor in cyclic stretching condition of up to 35 %.

2. Materials and methods

2.1. Materials

Photoresist AZ-5214E and formaldehyde was manufactured by Merck (Darmstadt, Germany), H2O2 by Technic (Staint Denis, France), NH4OH by T. Geyer GmbH (Rennigen, Germany), Poly(dimethylsiloXane) (PDMS) Sylgard 184 Silicone Elastomer Kit by Dow Corning Corp.

stage. Faust et al. developed such a versatile uniaxial stretching system

(Midland, RI, USA), (3-mercaptopropyl)trimethoXysilane (3MPTS),

with adjustable stretch frequency, amplitude and substrate stiffness that was used to investigate cell and cytoskeletal reorientation of human umbilical cord fibroblasts [47] and murine epithelial cell monolayers [48]. Furthermore, this group showed that cultivated cortical neurons react to stretch by directed cell growth and increased branching of dendrites [49].

In this context, the integration of electrical sensors into stretchable systems seems to be a highly promising approach for cell characterizations in real time. To date, stretched biological specimens are mainly characterized by optical methods. When combined with immunocytochemistry, these approaches only provide end-point measurements, which means that online monitoring with high temporal resolution is rarely possible and cells cannot be recovered after staining.

In contrast, electrical impedance spectroscopy (EIS) enables realtime, label-free, non-invasive analyses of cells and cell layers by their frequency-dependent dielectric properties. Electric cell-substrate impedance sensing (ECIS), pioneered by Giaever and Keese in 1984 [50], permits to draw functional insights from the electrical properties

Dulbecco's modified Eagle Medium (DMEM), glucose, trypsin, EDTA, penicillin/streptomycin solution by Sigma-Aldrich (St. Louis, MO, USA), fetal bovine serum by PAN Biotech (Aidenbach, Germany), and Bovine Serum Albumin (BSA) powder by Carl Roth (Karlsruhe, Germany) dissolved to 0.1 % and 1 % in phosphate buffered saline (PBS), respectively.

2.2. Methods

2.2.1. Cell culture chambers

The fabrication process was already presented in [59] and is briefly summarized in the following here: a photoresist layer of AZ-5214 with a layer thickness of 1.4 µm was spin-coated and prebaked on 4'' silicon wafers. The photoresist served as sacrificial layer. The front side of the wafers were subsequently sputtered with titanium (Ti, 50 nm) and gold (Au, 400 nm) and patterned by standard UV-lithography (MA6, Suss Microtec, Munich, Germany). After wafer-dicing, Au wires (diameter 50.8 µm) were micro-welded using a DC resistance welding system (HF25, Unitek Miyachi Corporation, USA) on Au contact pad areas.

Then, the chips were exposed to 3MPTS in the vapor phase at 25 ◦C for 30 min and cast with PDMS (precursor : curing agent 40:1 by weight) in a custom-made mold (negative of cell culture chamber) followed by a Cy3-633 secondary antibody (Goat REFA21071, Invitrogen, USA). All antibodies were used in a 1:200 dilution in CB. Antibodies were visualized on a confocal microscope (cLSM 880, Zeiss, Oberkochem, Gercuring step at 60 ◦C for 16 h. For the removal of the sacrificial photoresist and the detachment of the chip, the sample was immersed in dry ethanol for 72 h. At last, the remaining Ti adhesion layer was etched by H2O2, NH4OH and H2O solution (1:1:5 by volume).

many) with a Plan-Neofluar appropriate filter settings.

3. Results and discussion

40X/1.3

NA DIC oil objective and

3.1.1. Cell culturing

MDCK (Madin-Darby canine kidney) cells, which express a stably incorporated murine desmoglein 2-GFP, as well as A549 (human alveolar basal epithelial adenocarcinoma) cells were cultured in DMEM with high glucose concentrations (4.5 g/mL) supplemented with 10 % fetal bovine serum and 100 U/mL penicillin/streptomycin solution. Cells were detached using trypsin/EDTA. After detachment, cells were centrifuged at 200 g for 5 min and re-suspended in culture medium to the desired cell number.

For stretch experiments with MDCK cells, stretch chambers were coated with 20 µg/mL fibronectin (BD Biosciences, San Jos´e, CA, USA) in PBS for 1 h at 37 ◦C. Per chamber, 1.7 × 105 MDCK cells were seeded. Before stretching, cells were incubated for 5 days at 37 ◦C and 5% CO2 to form a dense monolayer.

For stretch experiments with A549 cells, stretch chambers were coated with 40 µg/mL collagen G for 1 h at 37 ◦C. Subsequently, 750 µl cell suspension with 8 × 105 cells/mL were added to each well. Before stretching, the cells were incubated for 3 days at 37 ◦C and 5% CO2 to form a dense monolayer.

For both cell cultures, the culture medium was exchanged every 24 h. The culture medium was carefully pipetted down at a corner of the chamber, without exposing the cell layer to air. Afterwards, new medium was pipetted up.

3.1.2. Stretch experiments and impedance measurements

Cell culture chambers were clamped into the 6-fold in-house developed uniaxial cell stretcher [15,55]. The Au wires were soldered on a printed circuit board (PCB), which was connected to an impedance spectrometer (ISX-5, Sciospec Scientific Instruments, Bennewitz, Germany) via SMB connectors. After the cell seeding and the development of a cell monolayer, a uniaxial static strain was applied as a stepwise increase from 0 % to 35 % in 5 % steps. The ramp-up to the stretched and the ramp-down to the original position were carried out with a velocity of 1 mm/s. 1 mm stretching corresponded to 5 % of the length of the non-stretched chamber. Each strain amplitude was maintained for 6 min. Between each amplitude, the stretch was released to zero also for 6 min. At each strain position, two impedance spectra (50 logarithmic steps between 100 Hz and 1 MHz) were recorded in three-minute intervals. For MDCK cell layers, the averaged impedance magnitudes were analyzed at a frequency of 19 kHz, whereas for A549 cell layers, averaged impedance magnitudes were evaluated at a frequency of 34 kHz, respectively. At these two frequencies, the corresponding cell type showed the highest impedance magnitudes with respect to values obtained without a cell layer above the electrodes. Measurements were related to a starting point at t 0 s, at which the impedance saturated after the cell monolayer growth and stretching was applied.

3.1.3. Immunocytochemistry

After the monolayer formation, MDCK cells were either stretched or grown without stretch for cell-cell contact analysis. Subsequently, cells were fiXed with 3.7 % formaldehyde in cytoskeleton buffer (CB; 150 mM NaCl, 5 mM MgCl2, 5 mM EGTA, 5 mM glucose, 10 mM 2-(N-morpho-

lino) ethanesulfonic acid, pH 6.1) at 37 ◦C for 10 min and further

handled as described before [62]. Desmosomes were visualized at 488 nm to illuminate the stably incorporated desmoglein 2-GFP. For actin staining, phalloidin 405 (Sigma Aldrich, USA) was used in a 1:200 dilution. Adherens junctions were visualized using a primary antibody against α-catenin (Rabbit C2081, Sigma Aldrich, USA) and an anti-rabbit

For the use in uniaxial stretcher setups, interdigitated electrodes have to be aligned perpendicularly to the stretching direction to prevent a fracture of the electrodes. This is an advantage compared to previous work [63], in which only microelectrode arrays were fabricated on stretchable PDMS. Using these wide-spaced electrodes, high-resolution ECIS measurements cannot be performed.

Electrodes were connected with stretchable meander-type conductor lines, as illustrated in Fig. 1. Meander-type conductor lines are necessary to prevent their fracture in the stretching direction. As described in our previous work [59], 20 µm wide gold meander with a radius (R) to width

(W) ratio (R/W ratio) of 3 turned out to be suitable for a balanced stretchability on 50 kPa PDMS. The finding of an appropriate junction to contact one electrode finger with the meander was assisted by using Finite Element Method (FEM) modeling, where different locations within the meander were investigated with respect to the criterion of maximum induced plastic strain, which is an indication of mechanical fatigue. As shown in Fig. 1a, large plastic strains can be effectively avoided by connecting the meander to the perpendicularly conjoined electrodes at maximum/minimum points of meander arcs. Details of our design consideration is further described in Figure S1.

A novel pattern made of networked meanders that matches the periodicity of the meander (320 µm) to the periodicity of the interdigitated electrodes (80 µm) was developed. Fig. 1b shows the fabricated design with 20 µm wide gold conductors and electrode lines on 50 kPa PDMS. Meander lines with R/W 3 were placed in parallel and interconnected to the electrodes at maximum/minimum points of meander arcs. Furthermore, novel horseshoe-like branches, which also induce very low plastic deformation as shown in Fig. 1a, were used as interposers to connect every second electrode. Multiple parallel-shifted

meanders support the interdigital electrodes as stretchable conductors. The networked meanders further ensure the robustness during stretching and decrease the electrical resistances of the conductor. During stretching, the interdigital electrodes expand homogeneously, increasing the distance between each other, as shown in Fig. 1c. The strain distribution between the electrodes caused by stretching is thus precisely aligned, which is highly favorable for exact uniaxial stretch [47]. At the very end of the meander conductor, gold wires are welded on the contact pad for electrical accessibility, as shown in Fig. 1d. Furthermore, the contact pads also adopt the meander design to accommodate excessive stress induced by stretching. The finger electrodes in the sensor area are 3.65 mm long. We note that the ECIS sensor is only designed to be stretched in one direction; in other directions, especially perpendicular to the designated stretch direction, both electrodes and meanders will experience large stress fracture.

The electrical access to the sensor element on a stretching PDMS

membrane is very challenging. To address this issue, the novel bonding strategy was developed. As illustrated in Fig. 2a, gold structures were first fabricated on top of a silicon chip covered with a polymeric sacrificial layer. Gold micro wires (50.8 µm diameter) were then microwelded to the gold pads before casting the PDMS in the mold. Etching of the sacrificial as well as the titanium layer released the chip and left the pristine gold microstructure embedded in PDMS substrate. It is worthwhile to note that the contact pad and the fiXed end of the gold wire were completely embedded in the PDMS substrate, while the other end of the gold wire can easily be connected, e.g. manually, to an impedance spectrometer. The novel bonding method excludes the environmental impact on gold wires and furthermore does not affect the flatness of the culturing membrane, which can ensure stable electrical contact over thousands of stretching cycles. The finished device that is transferred into PDMS is shown in Fig. 2b. This approach has also high potential for extending the scope of stretchable electronics into more three-dimensional systems.

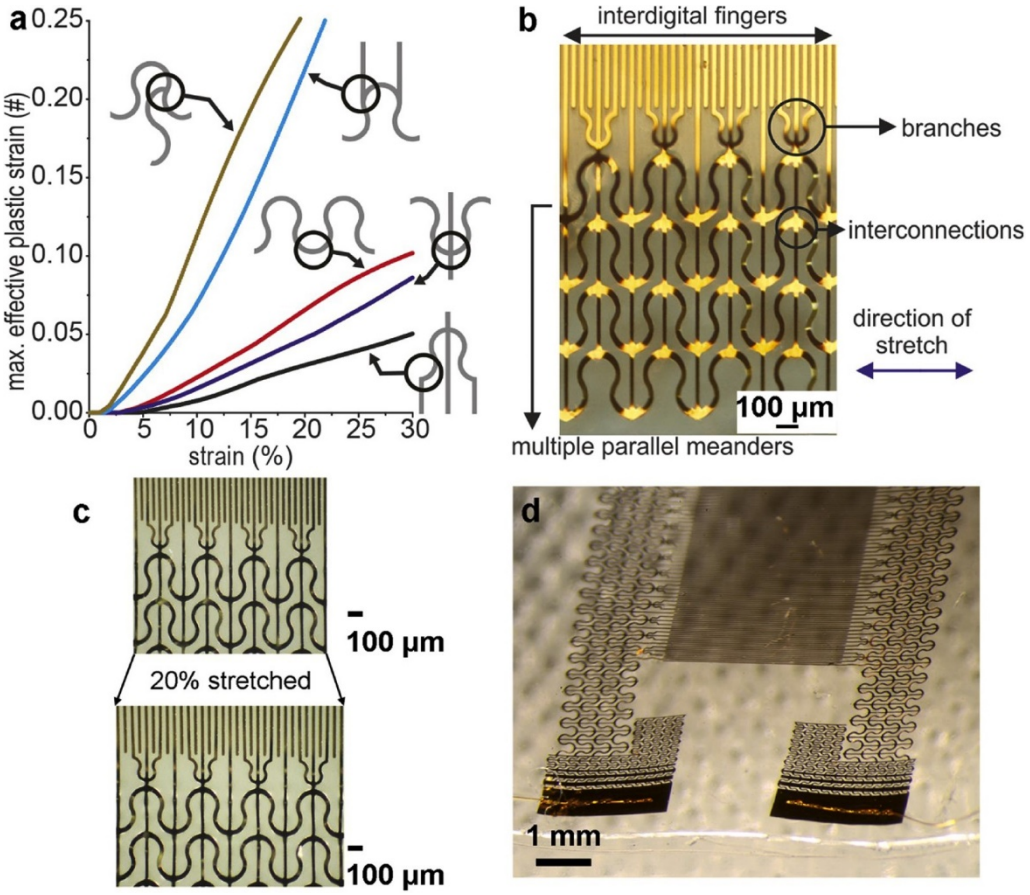

Fig. 1 Concept of interconnecting the closed-packed interdigitated electrodes for ECIS measurements with stretchable meander-type conductor lines: (a) Maximal effective plastic strain with respect to the applied strain for different interconnection positions. The FEM simulation results revealed the best performing interconnections between electrode and conductor meander by connecting the meander to the perpendicularly conjoined electrodes at maximum/minimum points of meander arcs (purple line). Even lower stress is present within branch structure (black line), which is however not an interconnection. (b) Photo of fabricated interdigitated electrodes with connected interlaced meander on ultra-elastic PDMS substrate and description of individual elements. (c) Original and 20 % stretched interdigitated electrodes. (d) Photo from the backside of interdigitated electrodes on PDMS substrate with meandered contact pads and welded gold wire.

Moreover, in order to prevent fatigue of the contact pad during extended stretching, the networked meander structure was also incorporated into the design of the contact pad, as shown in Fig. 2c. In order to be able to connect the pad with gold wires by the micro-welding technique, gold stripes with increasing width were integrated into the pads to manage the stress contribution.

Generally, the whole fabrication process offers great versatility in imitating well-defined environmental conditions by allowing fine-tuned PDMS elasticities with the help of suitable PDMS formulations. The tuning of the PDMS formulation directly yields different substrate and surface elasticities [47], posing a high versatility towards well-adjusted cell/substrate moduli [62,64]. Clearly, other stretchable elastomers can also be used if casting of these polymers into the mold is possible.

Assisted by the innovative contacting strategies of interlaced meanders and micro-welding, the stretchable interdigitated electrodes were at first characterized by impedance measurements without medium and with applied static strains from 0 % to 30 %, of which results are shown in Fig. 3a. An analytical calculation of the impedance was performed (details in Supplementary information) to compare with the experimental results. The good match between the measured impedance with our model indicates that the strain applied to the membrane is homogenously accommodated between the interdigitated electrodes. Furthermore, EIS measurements were carried out filling the chamber with phosphate-buffered saline (PBS) or bovine serum albumin (BSA) powder dissolved to 0.1 wt. % in PBS [65,66]. The results are shown in Fig. 3b and c for the amplitude and phase information at zero strain.

The impedance measurements were accompanied by fitting the

results to electric equivalent circuits. Here, physical properties can be assigned to different circuit elements [67,68]. As depicted in Fig. 3d, the electrode/electrolyte interface impedance can easily be modeled using a modified Randles circuit including the solution resistance (RSOL), the double-layer capacity (CPEDL) and the charge-transfer resistance (RCT). In addition, parasitic effects due to, e.g., wire bonds and leads, are considered by the constant phase element CPEPAR, the resistances and inductances of the leads by RLEAD and LLEAD, respectively. It is noteworthy that parasitic effects dominate only at higher frequencies. For data fitting, the Powell algorithm (1000 iterations) and the open-source software "EIS Spectrum Analyser" (http://www.abc.chemistry.bsu.by/ vi/analyser/) were used [69]. Obtained values of the circuit elements including relative errors are listed in Table S1 in the Supplementary information. RCT shows very high values due to the lack of redoX couples in the solution. Thus, only non-faradaic charge transfer occurs at the electrodes. Neglecting faradaic currents, the electrode/electrolyte

interface (dominating at lower frequencies) can be modeled by RSOL in series with CPEDL. The impedance of CPEDL is given by ZDL 1/[Q·(jω)n] where Q is the capacity of the double-layer, n the exponent of the CPE and ω 2π·f the angular frequency [70–72]. For monitoring BSA adsorption on the electrodes surface, the double-layer impedance at a low frequency is a decent measure. Therefore, the dependency of ZDL

values normalized to ZDL,PBS,0% strain on the applied strain are shown in Figure S2a in the Supplementary information for a frequency of 250 Hz. ZDL,PBS,0% strain equals 326.7 Ω in PBS without strain. After the applica-

tion of BSA, the impedance rises by a factor of 2.05 to ZDL,BSA,0% strain =

669.3 Ω. This jump is responsible for the curve shift to higher impedance

values after BSA-coverage, as shown in Fig. 3b. Thus, the developed sensor is sensitive towards the binding of biomolecules to the surface of the electrode, and the behavior electrode coverage can be explained by electric equivalent circuits.

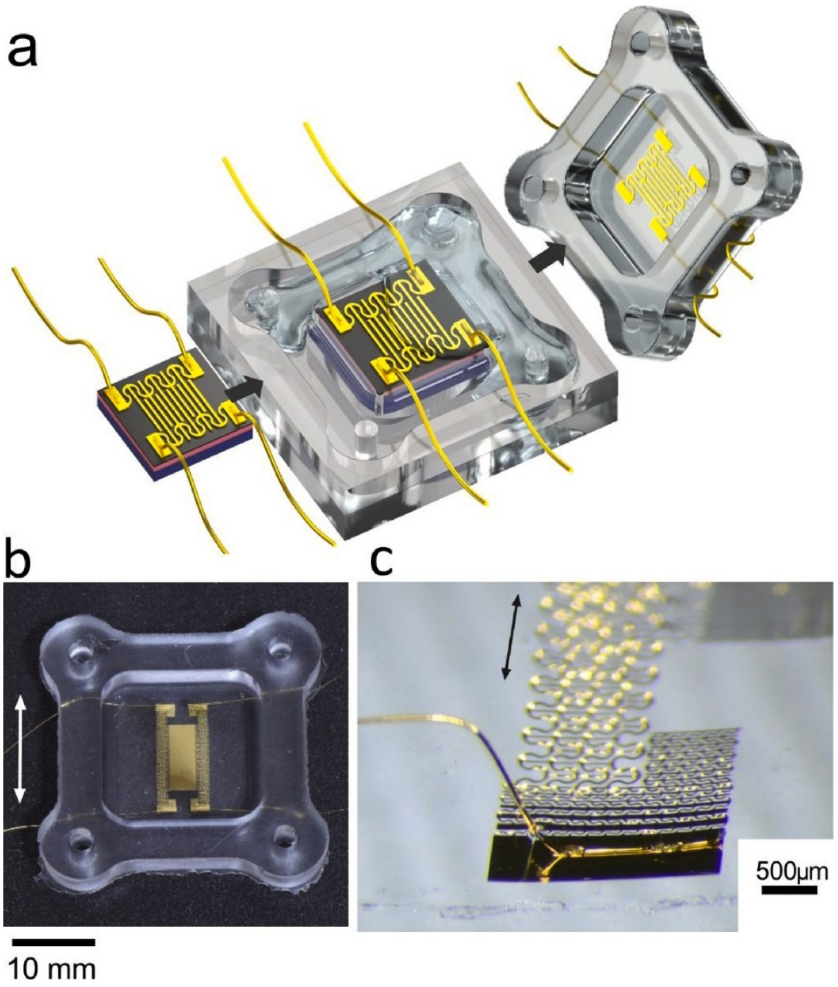

Fig. 2 3D Illustration of the stretchable ECIS sensor fabrication process: (a) Gold microstructures were fabricated on a silicon chip with a polymer-based sacrificial layer while gold wires were micro-welded onto the contact pads. The sensor was then cast in PDMS followed by removing the polymer sacrificial layer as well the Ti layer, leaving pure gold structure embedded in PDMS substrate. (b) Photo of gold pad on the silicon chip with micro-welded gold wire. (c) Photo of detail of the final device taken from the backside of the PDMS membrane showing microstructures in the back, gold pad in front with micro welded gold wire penetrating through the transparent PDMS substrate. In (b)-(c) the stretch direction is indicated with an arrow.

Subsequent stretching of the BSA primed sensor to static strains of 10

% (ZDL,BSA,10 % strain 667.4 Ω) and 20 % (ZDL,BSA,20 % strain 671.4 Ω)

leads only to minor additional changes in the double-layer capacity value. These minor deviations are within the uncertainty of the fitted circuit elements (compare Table S1). The build-up of a double-layer capacity is a near-surface effect at the electrodes and is not influenced by stretching of the membrane. Worthwhile to note, RSOL increases only by values in the mΩ-range when strain is applied, as shown exemplarily for the BSA-coated sensor in Figure S2b in the Supplementary information. The negligible rise is due to the enlarged distance between the electrodes. These results reveal impressively that stretching the sensor in PBS or in PBS with BSA-coating does not affect the EIS signals significantly.

To characterize long-term stretch tests, the developed devices were clamped into a 6-fold uniaxial cell stretcher [73], as shown in Figure S4 in the Supplementary information. The stretching behavior of the membrane with integrated interdigital electrodes is shown in the video as Figure S5 in the Supplementary information. For this work, cyclic stretch tests of 20 % and 30 % were carried out with a stretch-and-release frequency of 1 Hz to characterize the long-term performance. 10,000 cycles were performed. During these cyclic stretching tests, a pre-stretch of 7.5 % relative elongation was applied.

It was assumed that this pre-stretch would compensate the bending of the chamber's bottom by the weight of the cell culture medium during cell experiments, but it was not confirmed by the later experiments. The electrical resistance was measured by contacting one networked meander. The cyclic strain of 20 % increased the electrical resistance by only 0.4 %. This small increase is not critical for the characterization of

the electrical impedance, since high DC impedances are always present due to the electrical double layer at the electrode/electrolyte interface. Similarly, the impedance profile of the EIS electrode does not change significantly when stretched up to 18 h in BSA/PBS solution, as shown in Figure S2. When the stretching amplitude stepped up to 30 %, the relative change in resistance increased to 10 %, indicating a certain degree of fatigue in the interconnections of the conductor. However, 100

% of the networked meander conductors remained electrically conductive, unlike the single meander structure shown in our previous work [59].

For proof-of-concept, epithelial Madin-Darby canine kidney (MDCK) cells, which are well-known for forming a tight monolayer and well used for permeability analyses, were seeded and cultured in the device. They formed a tight monolayer of highly cylindrical cells with matured intercellular contacts (desmosomes and adherens junctions), as indicated in Fig. 4a by visualization of a stably incorporated murine desmoglein 2-GFP and immunocytochemistry staining of adherens junctions via α-catenin.

To monitor MDCK layers under stretching conditions, uniaxial static

stretch amplitude was increased from 0 % to 35 % in 5 % steps. Strain was held constant for 6 min and then released to 0 % with an additional waiting time of 6 min. On a local (i.e. cellular) scale, stretch occurs mostly at the soft elastomer areas in between the more rigid interdigitated gold fingers. Interestingly, MDCK cells displayed a strongly reduced number of actin filaments at these soft regions (Fig. 4b) indicating a clear cytoskeletal response.

Simultaneously to stretching, ECIS experiments were performed, which are summarized in Fig. 5. The mean values of the magnitudes of the impedance in the released state after application of a certain strain | Zreleased| are referred to the magnitudes of impedance at the starting point of the experiment at t 0 s |Zt 0s|, This ratio is plotted with respect to the applied strain value.

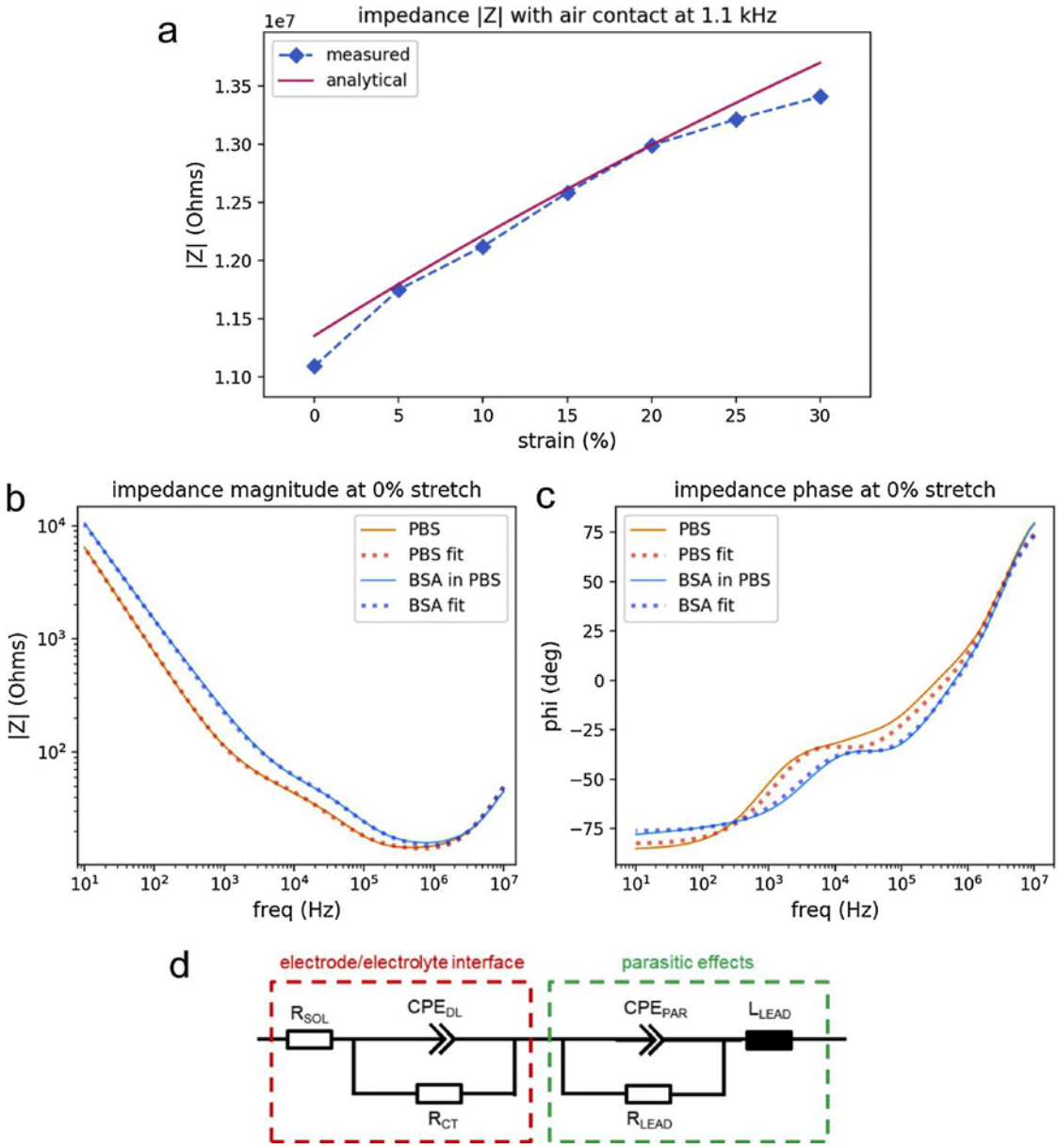

Fig. 3. Impedance measurements on stretchable interdigitated electrodes without cell monolayer. (a) Magnitude of the impedance with air contact at different strain levels. (b), (c) Magnitude and phase of the impedance of the ECIS electrode at 0 % strain measured with phosphate-buffered saline (PBS) solution or bovine serum albumin (BSA) powder dissolved to 0.1 % in PBS. (d) Electric equivalent circuit modeling the electrode/electrolyte interface (dashed red boX) as well as parasitic effects due to the measurement setup (dashed green boX).

Interestingly, impedance increased significantly for MDCK monolayers at strain amplitudes above 20 %. The staining for actin of MDCK monolayers after stretch indicates a rupture of actin filaments inside the cells only at sites of PDMS elastomer between the interdigitated gold fingers (Fig. 4b). In contrast, actin filaments in cells above the nonstretchable gold surface appeared unaffected. Irrespective of the location, cell-cell contacts seemed unaffected. As actomyosin is the force generating system of cells, these observations might indicate a relaxed state for intercellular contacts after strains with amplitudes above 20 %. As a consequence, one would expect lowered distances between cells, which would be in line with the impedance increase above this strain level.

These results are in good agreement with stability measurements for the main cytoskeletal systems, i.e., actin and intermediate filaments, attached to cell-cell contacts [47,74,75]. In those experiments, it was found that the structure of the actin cytoskeleton changed dramatically at identical strain amplitudes as used here while intermediate filaments remained stable even for strain amplitudes above 100 %. Reorganization of the actin cytoskeleton as response to both signals, stretch and stiffness, are well documented [76–79].

For comparison, we cultivated A549 monolayers that lack mature cell junctions and therefore do not develop a permeability barrier. Fig. 5 shows |Zreleased|/|Zt=0s| values at a frequency of 34 kHz. In contrast to MDCK monolayers, A549 monolayers showed a continuous decrease of impedance over the whole range of applied strain.

In the past, impedance measurements and immunohistochemistry have repeatedly shown that A549 cells in a monolayer do not develop tight junctions or polarity [79–82]. Thus, the tight junction protein impedance were seen. Instead, the impedance increases gradually with applied strain in case of the MDCK cell layer, whereas for the A549 cell layer, the impedance decreases continuously with increasing strain without any leaps.

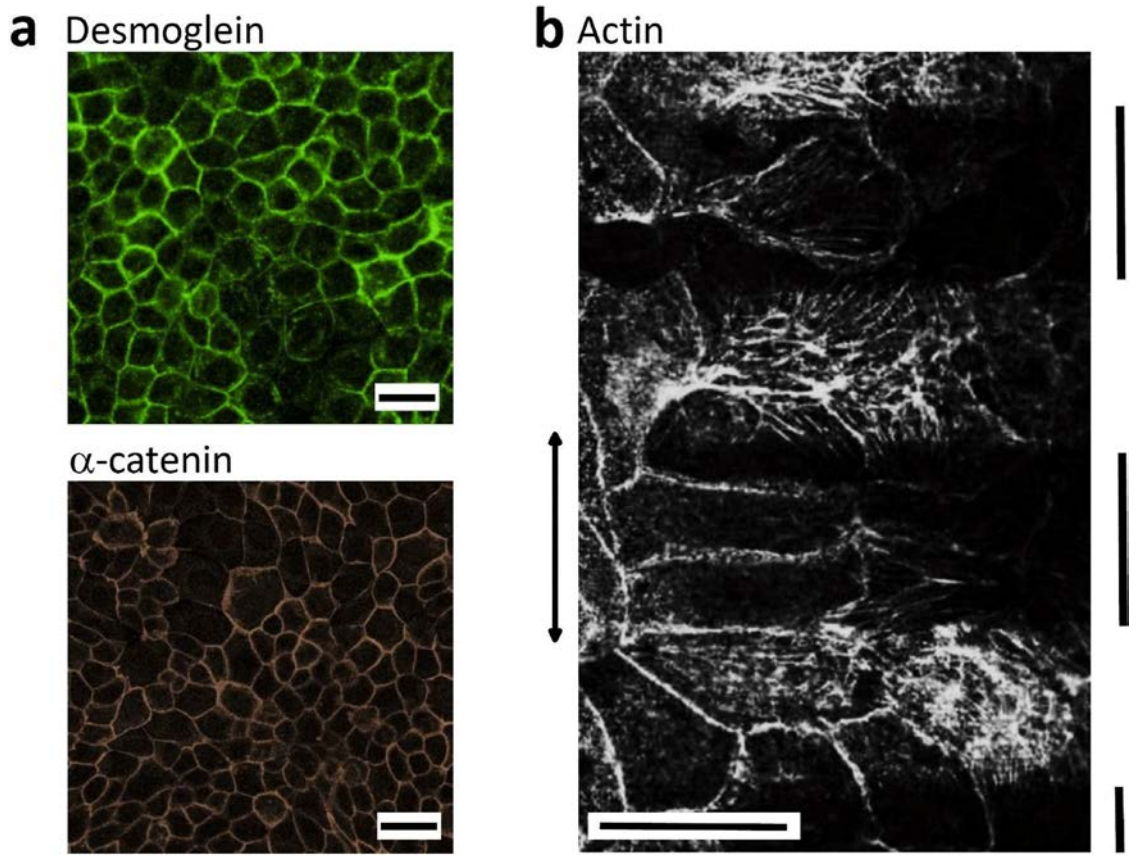

Fig. 4. Microscopic images of cultivated cell monolayers: (a) MDCK cell monolayers on stretchable membranes with interdigital electrodes were fiXed and visualized for desmosomes (desmoglein 2-GFP) and adherens junctions (α-catenin). (b) Monolayers were stained for actin after the last 35 % strain and analyzed in the center of the stretching chamber at sites of interdigitated gold fingers. Elastomer areas in between of the electrodes are indicated by black lines (right). Note the reduction of actin filaments in stretched PDMS areas. The stretch direction is indicated by the arrow on the left. Scale bars in (a) and (b): 20 µm.

4. Conclusions

We presented the development of a versatile platform for uniaxial cell monolayer stretching that combines tunable substrate stiffness, densely packed interdigital microelectrodes, highly stretchable meander-type feed lines, and reliable electrical contacting strategies on stretchable substrates. The system provides the capability of reliable continuous long-term monitoring of electrical properties of cell monolayers by surface-sensitive electrical cell-substrate impedance spectroscopy even above physiological strain values of epithelial cell cultures, zonula occludens 1 (ZO1) and the adherence junction protein E-cadherin (epithelial cadherin) are only expressed rudimentarily or not at all [82, 83]. In the stretching experiments performed here, a continuous decrease in impedance was detected in response to applied strain. This could be due to the fact that A549 cells still express desmoplakin, which indicates intact desmosomes between the cells that might have been stressed by the strain [82].

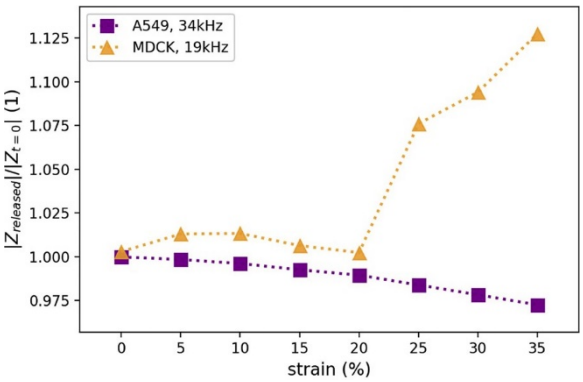

Fig. 5 Fig. 5. ECIS measurements. Magnitudes of the impedance in the released state

after application of a certain strain |Zreleased| referred to the magnitudes of impedance at t = 0 s |Zt=0s| are plotted with respect to the applied strain values. Plotted are the mean values. ECIS measurements were carried out at 19 kHz for MDCK and at 34 kHz for A549 lung epithelial cell monolayers, respectively.

For both cell types, it can be assumed that strain application up to 35% did not lead to a rupture of the cell layers, as no abrupt changes in which were investigated. Although the developed platform is not suitable for high-throughput screening applications and cannot be used in arrangements such as 96 or 384 well plate formats, the use of a 6-fold uniaxial stretcher indicates that screening at a low level is possible. The advantage of the setup is that it is possible to adjust the stiffness of the membrane to physiological relevant stiffness of the investigated cell monolayer by simple casting corresponding composed PDMS into the mold. It was demonstrated that the developed setup has the potential to pick up cell-specific differences in cell monolayer behavior. Importantly, following impedance spectroscopic analysis, cells are still alive and can be used for further experiments or can be harvested for additional analyses like genetic or proteomic screens. Furthermore, monitoring of epithelial permeability changes in real time to screen the influence of pharmacological substances is expected to be of high academic and industrial interest. The advantage of the introduced platform is that label-free and non-destructive electrical near-surface measurements can be carried out. On the other hand, general innovations emerging within the system like interlaced meander and embedded micro-wiring are also holding great promise to catalyze further innovations in stretchable electronics.

Author contributions CZ designed the concept and ECIS sensor layout and developed the fabrication technology, SB optimized the fabrication technology and carried out ECIS experiments. CZ did FEM simulations. SB and TK carried out data analysis. CH and SG performed all cell experiments on MDCK cells, whereas AB was responsible for A 549 cell culturing experiments. BH and RM developed the cell stretcher and designed the experiments on cellular level. AL, SU and US supervised the project. All authors, except CH, SG and SU contributed to the manuscript. All authors have given approval to the final version of the manuscript.

CRediT authorship contribution statement

Chen Zhou: Conceptualization, Investigation, Formal analysis, Data curation, Validation, Visualization, Writing original draft. Sebastian Bette: Investigation, Validation, Visualization, Formal analysis, Data curation, Software, Writing original draft. Aaron Babendreyer: Conceptualization, Investigation, Formal analysis, Data curation, Validation, Writing original draft. Christina Hoffmann: Investigation, Validation, Visualization, Formal analysis, Data curation. Sven Gerlach: Investigation, Validation, Visualization, Formal analysis, Data curation. Tom Kremers: Formal analysis, Visualization, Writing original draft. Andreas Ludwig: Methodology, Writing review & editing, Project administration, Funding acquisition. Bernd Hoffmann: Methodology, Writing original draft. Rudolf Merkel: Supervision, Writing review & editing, Project administration, Funding acquisition. Stefan Uhlig: Supervision, Writing review & editing, Funding acquisition. Uwe Schnakenberg: Supervision, Writing review & editing, Project administration, Funding acquisition.

Declaration of Competing Interest

The authors report no declarations of interest.

Acknowledgment

The work was partly funded by the EXcellence Initiative of the German federal and state governments [grant OPBF071-MechCell] and the Deutsche Forschungsgemeinschaft (DFG, German Research Foundation) HO2384/2 and ME1458/8 within SPP1782 as well as 363055819/GRK2415. CZ, SB and US express their serious thanks to Dorothee Breuer, Ewa-Janina Sekula, Jochen Heiss, and Suthanthiran Pulenthiran for their assistance in device processing. AL, SU, and US acknowledge Dr. Elke Müller for her extraordinary engagement in supporting the research field “Mechanobiology” at RWTH Aachen University. US acknowledges Linda Wetzel for careful proof-reading of the manuscript. We also thank Prof. Rudolf Leube (MOCA, RWTH Aachen University) for providing us with the stably transfected murine Desmoglein2-GFP MDCK cells.

Appendix A. Supplementary data

Supplementary material related to this article can be found, in the online version, at doi:https://doi.org/10.1016/j.snb.2021.129656.

References

[1] A.J. Bandodkar, J. Wang, Non-invasive wearable electrochemical sensors: a review, Trends Biotechnol. 32 (2014) 363–371.

[2] A. Economou, C. Kokkinos, M. Prodromidis, Flexible plastic, paper and textile labon-a chip platforms for electrochemical biosensing, Lab Chip 18 (2018) 1812–1830.

[3] P. Kumari, L. Mathew, P. Syal, Increasing trend of wearables and multimodal interface for human activity monitoring: a review, Biosens. Bioelectron. 90 (2017) 298–307.

[4] J.M. Peake, G. Kerr, J.P. Sullivan, A critical review of consumer wearables, mobile applications, and equipment for providing biofeedback, monitoring stress, and sleep in physically active populations, Front. Physiol. 9 (2018) 743.

[5] P.B. Shull, D.D. Damian, Haptic wearables as sensory replacement, sensory augmentation and trainer–a review, J. Neuroeng. Rehabil. 12 (2015) 59.

[6] I.R. Minev, P. Musienko, A. Hirsch, Q. Barraud, N. Wenger, E.M. Moraud, et al., Electronic dura mater for chronic multimodal neural interfaces, Science 347 (2015)

159–163.

[7] J. Bloch, S.P. Lacour, G. Courtine, Electronic dura mater meddling in the central nervous system, JAMA Neurol. 74 (2017) 470–475.

[8] J.A. Fan, W.-H. Yeo, Y. Su, Y. Hattori, W. Lee, S.-Y. Jung, et al., Fractal design concepts for stretchable electronics, Nat. Commun. 5 (2014) 1–8.

[9] R.C. Webb, A.P. Bonifas, A. Behnaz, Y. Zhang, K.J. Yu, H. Cheng, et al., Ultrathin conformal devices for precise and continuous thermal characterization of human skin, Nat. Mater. 12 (2013) 938–944.

[10] D.-H. Kim, N. Lu, R. Ma, Y.-S. Kim, R.-H. Kim, S. Wang, et al., Epidermal electronics, Science 333 (2011) 838–843.

[11] L. Xu, S.R. Gutbrod, Y. Ma, A. Petrossians, Y. Liu, R.C. Webb, et al., Materials and fractal designs for 3D multifunctional integumentary membranes with capabilities in cardiac electrotherapy, Adv. Mater. 27 (2015) 1731–1737.

[12] D. Ingber, Mechanobiology and diseases of mechanotransduction, Ann. Med. 35 (2003) 564–577.

[13] J.H.-C. Wang, B.P. Thampatty, An introductory review of cell mechanobiology, Biomech. Model. Mechanobiol. 5 (2006) 1–16.

[14] D.-H. Kim, P.K. Wong, J. Park, A. Levchenko, Y. Sun, Microengineered platforms for cell mechanobiology, Annu. Rev. Biomed. Eng. 11 (2009) 203–233.

[15] M.J. Yost, D. Simpson, K. Wrona, S. Ridley, H.J. Ploehn, T.K. Borg, et al., Design and construction of a uniaxial cell stretcher, Am. J. Physiol.-Heart Circul. Physiol. 279 (2000) H3124–H3130.

[16] G. Bartalena, R. Grieder, R.I. Sharma, T. Zambelli, R. Muff, J.G. Snedeker, A novel method for assessing adherent single-cell stiffness in tension: design and testing of

a substrate-based live cell functional imaging device, Biomed. Microdevices 13 (2011) 291–301.

[17] J.H.-C. Wang, P. Goldschmidt-Clermont, F.C.-P. Yin, Contractility affects stress fiber remodeling and reorientation of endothelial cells subjected to cyclic mechanical stretching, Ann. Biomed. Eng. 28 (2000) 1165–1171.

[18] O. Aydin, B. Aksoy, O. Akalin, H. Bayraktar, B. Alaca, Time-resolved local strain tracking microscopy for cell mechanics, Rev. Sci. Instrum. 87 (2016) 023905.

[19] Y. Shao, X. Tan, R. Novitski, M. Muqaddam, P. List, L. Williamson, et al., Uniaxial cell stretching device for live-cell imaging of mechanosensitive cellular functions, Rev. Sci. Instrum. 84 (2013) 114304.

[20] S. Iwayoshi, K. Furukawa, T. Ushida, Continuous visualization of morphological changes in endothelial cells in response to cyclic stretch, JSME Int. J., Ser. C 49 (2006) 545–555.

[21] K. Kurpinski, J. Chu, C. Hashi, S. Li, Anisotropic mechanosensing by mesenchymal stem cells, Proc. Natl. Acad. Sci. 103 (2006) 16095–16100.

[22] J. Zhuang, K.A. Yamada, J.E. Saffitz, A.G. Kl´eber, Pulsatile stretch remodels cell-to-

cell communication in cultured myocytes, Circ. Res. 87 (2000) 316–322.

[23] M. Liu, S. Montazeri, T. Jedlovsky, R. Van Wert, J. Zhang, R.-K. Li, et al., Biostretch, a computerized cell strain apparatus for three-dimensional organotypic cultures, in vitro cell, Dev. Biol. Anim. 35 (1999) 87–93.

[24] S. Seriani, G. Del Favero, J. Mahaffey, D. Marko, P. Gallina, C. Long, et al., The cellstretcher: a novel device for the mechanical stimulation of cell populations, Rev. Sci. Instrum. 87 (2016) 084301.

[25] D. Huh, B.D. Matthews, A. Mammoto, M. Montoya-Zavala, H.Y. Hsin, D.E. Ingber, Reconstituting organ-level lung functions on a chip, Science 328 (2010) 1662–1668.

[26] R. Kaunas, P. Nguyen, S. Usami, S. Chien, Cooperative effects of Rho and mechanical stretch on stress fiber organization, Proc. Natl. Acad. Sci. 102 (2005) 15895–15900.

[27] S. Deguchi, S. Kudo, T.S. Matsui, W. Huang, M. Sato, Piezoelectric actuator-based cell microstretch device with real-time imaging capability, AIP Adv. 5 (2015), 067110.

[28] K. Sato, S. Kamada, K. Minami, Development of microstretching device to evaluate cell membrane strain field around sensing point of mechanical stimuli, Int. J. Mech.

Sci. 52 (2010) 251–256.

[29] Y. Iwadate, C. Okimura, K. Sato, Y. Nakashima, M. Tsujioka, K. Minami, Myosin-IImediated directional migration of Dictyostelium cells in response to cyclic stretching of substratum, Biophys. J. 104 (2013) 748–758.

[30] K. Nagayama, Y. Kimura, N. Makino, T. Matsumoto, Strain waveform dependence of stress fiber reorientation in cyclically stretched osteoblastic cells: effects of

viscoelastic compression of stress fibers, Am. J. Physiol. Cell Physiol. 302 (2012) C1469–C1478.

[31] F. Winston, E. Macarak, S. Gorfien, L. Thibault, A system to reproduce and quantify the biomechanical environment of the cell, J. Appl. Physiol. 67 (1989) 397–405.

[32] J. Gilbert, P. Weinhold, A. Banes, G. Link, G. Jones, Strain profiles for circular cell culture plates containing flexible surfaces employed to mechanically deform cells in vitro, J. Biomech. 27 (1994) 1169–1177.

[33] J. Williams, J. Chen, D. Belloli, Strain fields on cell stressing devices employing clamped circular elastic diaphragms as substrates, J. Biomech. Eng. 114 (1992) 377–384.

[34] A.J. Banes, J. Gilbert, D. Taylor, O. Monbureau, A new vacuum-operated stressproviding instrument that applies static or variable duration cyclic tension or compression to cells in vitro, J. Cell. Sci. 75 (1985) 35–42.

[35] J.L. Schaffer, M. Rizen, G.J. L'Italien, A. Benbrahim, J. Megerman, L.

C. Gerstenfeld, et al., Device for the application of a dynamic biaxially uniform and isotropic strain to a flexible cell culture membrane, J. Orthop. Res. 12 (1994) 709–719.

[36] F. Bieler, C. Ott, M. Thompson, R. Seidel, S. Ahrens, D. Epari, et al., Biaxial cell stimulation: a mechanical validation, J. Biomech. 42 (2009) 1692–1696.

[37] A. Colombo, P. Cahill, C. Lally, An analysis of the strain field in biaxial Flexcell membranes for different waveforms and frequencies, Proc. Inst. Mech. Eng., Part H 222 (2008) 1235–1245.

[38] X. Trepat, M. Grabulosa, F. Puig, G.N. Maksym, D. Navajas, R. Farr´e, Viscoelasticity

of human alveolar epithelial cells subjected to stretch, Am. J. Physiol. Lung Cell Mol. Physiol. 287 (2004) L1025–L1034.

[39] D. Wang, Y. Xie, B. Yuan, J. Xu, P. Gong, X. Jiang, A stretching device for imaging real-time molecular dynamics of live cells adhering to elastic membranes on inverted microscopes during the entire process of the stretch, Integr. Biol. 2 (2010) 288–293.

[40] H. Majd, P.J. Wipff, L. Buscemi, M. Bueno, D. Vonwil, T.M. Quinn, et al., A novel method of dynamic culture surface expansion improves mesenchymal stem cell proliferation and phenotype, Stem Cells 27 (2009) 200–209.

[41] A.A. Lee, T. Delhaas, L.K. Waldman, D.A. MacKenna, F.J. Villarreal, A.

D. McCulloch, An equibiaxial strain system for cultured cells, Am. J. Physiol., Cell Physiol. 271 (1996) C1400–C1408.

[42] C. Hung, J. Williams, A method for inducing equi-biaxial and uniform strains in elastomeric membranes used as cell substrates, J. Biomech. 27 (1994) 227–232.

[43] M. Sotoudeh, S. Jalali, S. Usami, J.Y. Shyy, S. Chien, A strain device imposing

dynamic and uniform equi-biaxial strain to cultured cells, Ann. Biomed. Eng. 26 (1998) 181–189.

[44] D. Ahrens, W. Rubner, R. Springer, N. Hampe, J. Gehlen, T.M. Magin, et al.,

A combined AFM and lateral stretch device enables microindentation analyses of living cells at high strains, Methods Protoc. 2 (2019) 43.

[45] J.P.V. Geest, E.S. Di Martino, D.A. Vorp, An analysis of the complete strain field within FlexercellTM membranes, J. Biomech. 37 (2004) 1923–1928.

[46] A. Dan, R.B. Huang, D.E. Leckband, Dynamic imaging reveals coordinate effects of cyclic stretch and substrate stiffness on endothelial integrity, Ann. Biomed. Eng. 44 (2016) 3655–3667.

[47] U. Faust, N. Hampe, W. Rubner, N. Kirchgessner, S. Safran, B. Hoffmann, et al., Cyclic stress at mHz frequencies aligns fibroblasts in direction of zero strain, PLoS One 6 (2011), e28963.

[48] B. Noethel, L. Ramms, G. Dreissen, M. Hoffmann, R. Springer, M. Rübsam, et al., Transition of responsive mechanosensitive elements from focal adhesions to adherens junctions on epithelial differentiation, Mol. Biol. Cell 29 (2018)

2317–2325.

[49] J.-A. Abraham, C. Linnartz, G. Dreissen, R. Springer, S. Blaschke, M.A. Rueger, et al., Directing neuronal outgrowth and network formation of rat cortical neurons by cyclic substrate stretch, Langmuir 35 (2018) 7423–7431.

[50] I. Giaever, C.R. Keese, Monitoring fibroblast behavior in tissue culture with an applied electric field, Proc. Natl. Acad. Sci. 81 (1984) 3761–3764.

[51] C.-M. Lo, C.R. Keese, I. Giaever, Impedance analysis of MDCK cells measured by electric cell-substrate impedance sensing, Biophys. J. 69 (1995) 2800–2807.

[52] H.T.N. Le, J. Kim, J. Park, S. Cho, A review of electrical impedance characterization of cells for label-free and real-time assays, Biochip J. 13 (2019) 295–305.

[53] J. Wegener, C.R. Keese, I. Giaever, Electric cell–substrate impedance sensing (ECIS)

as a noninvasive means to monitor the kinetics of cell spreading to artificial surfaces, EXp. Cell Res. 259 (2000) 158–166.

[54] S. Arndt, J. Seebach, K. Psathaki, H.-J. Galla, J. Wegener, Bioelectrical impedance assay to monitor changes in cell shape during apoptosis, Biosens. Bioelectron. 19 (2004) 583–594.

[55] J.M. Atienza, J. Zhu, X. Wang, X. Xu, Y. Abassi, Dynamic monitoring of cell adhesion and spreading on microelectronic sensor arrays, J. Biomol. Screening 10 (2005) 795–805.

[56] I. Giaever, C.R. Keese, Micromotion of mammalian cells measured electrically, Proc. Natl. Acad. Sci. 88 (1991) 7896–7900.

[57] P.O. Bagnaninchi, N. Drummond, Real-time label-free monitoring of adiposederived stem cell differentiation with electric cell-substrate impedance sensing, Proc. Natl. Acad. Sci. 108 (2011) 6462–6467.

[58] R. Szulcek, H.J. Bogaard, G.P. van Nieuw Amerongen, Electric cell-substrate impedance sensing for the quantification of endothelial proliferation, barrier function, and motility, J. Vis. EXp. (2014), e51300.

[59] C. Zhou, S. Bette, U. Schnakenberg, Flexible and stretchable gold microstructures on extra soft poly (dimethylsiloXane) substrates, Adv. Mater. 27 (2015) 6664–6669.

[60] S. MacKay, P. Hermansen, D. Wishart, J. Chen, Simulations of interdigitated electrode interactions with gold nanoparticles for impedance-based biosensing applications, Sensors 15 (2015) 22192–22208.

[61] P. Van Gerwen, W. Laureyn, W. Laureys, G. Huyberechts, M.O. De Beeck, K. Baert, et al., Nanoscaled interdigitated electrode arrays for biochemical sensors, Sens. Actuators B 49 (1998) 73–80.

[62] N. Hersch, B. Wolters, G. Dreissen, R. Springer, N. Kirchgeßner, R. Merkel, et al.,

The constant beat: cardiomyocytes adapt their forces by equal contraction upon environmental stiffening, Biol. Open 2 (2013) 351–361.

[63] I. Minev, S. Lacour, Impedance spectroscopy on stretchable microelectrode arrays, Appl. Phys. Lett. 97 (2010) 043707.

[64] A.J. Engler, S. Sen, H.L. Sweeney, D.E. Discher, MatriX elasticity directs stem cell lineage specification, Cell 126 (2006) 677–689.

[65] J. Lazar, M. Bialon, C. Püttmann, C. Stein, W. Germeraad, U. Schnakenberg, Multielectrode microfluidic platform for protein detection using electrochemical impedance spectroscopy, Clin. Technol. 45 (2015) 105–109.

[66] J. Lazar, R.R. Rosencrantz, L. Elling, U. Schnakenberg, Simultaneous electrochemical impedance spectroscopy and localized surface plasmon resonance

in a microfluidic chip: new insights into the spatial origin of the signal, Anal. Chem. 88 (2016) 9590–9596.

[67] T. Kremers, M. Tintelott, V. Pachauri, X.T. Vu, S. Ingebrandt, U. Schnakenberg, Microelectrode combinations of gold and polypyrrole enable highly stable twoelectrode electrochemical impedance spectroscopy measurements under turbulent flow conditions, Electroanalysis 32 (2020).

[68] T. Kremers, N. Menzel, F. Freitag, D. Laaf, V. Heine, L. Elling, et al., Electrochemical impedance spectroscopy using interdigitated gold–polypyrrole electrode combination, Physica Status Solidi A 217 (2020).

[69] A.S. Bondarenko, G.A. Ragoisha, Variable Mott-Schottky plots acquisition by potentiodynamic electrochemical impedance spectroscopy, J. Solid State Electrochem. 9 (2005) 845–849.

[70] J. Bisquert, G. Garcia-Belmonte, P. Bueno, E. Longo, L. Bulhoes, Impedance of constant phase element (CPE)-blocked diffusion in film electrodes, J. Electroanal. Chem. 452 (1998) 229–234.

[71] J.R. Macdonald, Note on the parameterization of the constant-phase admittance element, Solid State Ion. 13 (1984) 147–149.

[72] S.-B. Yoon, J.-P. Jegal, K.C. Roh, K.-B. Kim, Electrochemical impedance spectroscopic investigation of sodium ion diffusion in MnO2 using a constant phase element active in desired frequency ranges, J. Electrochem. Soc. 161 (2014)

H207–H213.

[73] Y. Kubo, B. Hoffmann, K. Goltz, U. Schnakenberg, H. Jahr, R. Merkel, et al., Different frequency of cyclic tensile strain relates to anabolic/catabolic conditions consistent with immunohistochemical staining intensity in tenocytes, Int. J. Mol. Sci. 21 (2020) 1082.

[74] D. Fudge, D. Russell, D. Beriault, W. Moore, E.B. Lane, A.W. Vogl, The intermediate filament network in cultured human keratinocytes is remarkably extensible and resilient, PLoS One 3 (2008) e2327.

[75] P.A. Janmey, U. Euteneuer, P. Traub, M. Schliwa, Viscoelastic properties of vimentin compared with other filamentous biopolymer networks, J. Cell Biol. 113 (1991) 155–160.

[76] A.J. Engler, M.A. Griffin, S. Sen, C.G. Bo¨nnemann, H.L. Sweeney, D.E. Discher, Myotubes differentiate optimally on substrates with tissue-like stiffness pathological implications for soft or stiff microenvironments, J. Cell Biol. 166

(2004) 877–887.

[77] K. Hayakawa, N. Sato, T. Obinata, Dynamic reorientation of cultured cells and stress fibers under mechanical stress from periodic stretching, EXp. Cell Res. 268 (2001) 104–114.

[78] R. Krishnan, C.Y. Park, Y.-C. Lin, J. Mead, R.T. Jaspers, X. Trepat, et al., Reinforcement versus fluidization in cytoskeletal mechanoresponsiveness, PLoS One 4 (2009) e5486.

[79] M.I. Hermanns, R.E. Unger, K. Kehe, K. Peters, C.J. Kirkpatrick, Lung epithelial cell lines in coculture with human pulmonary microvascular endothelial cells: development of an alveolo-capillary barrier in vitro, Lab. Invest. 84 (2004)

736–752.

[80] A. Carterson, K.H. Zu Bentrup, C. Ott, M. Clarke, D. Pierson, C. Vanderburg, et al., A549 lung epithelial cells grown as three-dimensional aggregates: alternative tissue culture model for Pseudomonas aeruginosa pathogenesis, Infect. Immun. 73 (2005) 1129–1140.

[81] H. Ren, N.P. Birch, V. Suresh, An optimised human cell culture model for alveolar epithelial transport, PLoS One 11 (2016), e0165225.

[82] J. Thompson, Cell lines of pulmonary and non-pulmonary origin as tools to study the effects of house dust mite proteinases on the regulation of epithelial permeability, Clin. EXp. Allergy 28 (1998) 1273–1285.

[83] A.D. Lehmann, N. Daum, M. Bur, C.-M. Lehr, P. Gehr, B.M. Rothen-Rutishauser, An in vitro triple cell co-culture model with primary cells mimicking the human alveolar epithelial barrier, Eur. J. Pharm. Biopharm. 77 (2011) 398–406.

Chen Zhou studied electrical engineering and computer science at RWTH Aachen University and continued working at Institute of Materials in Electrical Engineering 1 (IWE1) on magnetic tweezers, stretchable electronics, impedance spectroscopy and microfluidics. He received his PhD degree from Technical University Denmark in 2018 on optofluidics for life science applications.

Sebastian Bette studied physics and electrical engineering / micro systems technology at RWTH Aachen University. After graduation with a degree of Dipl.-Phys., he worked as a PhD student in Prof. Schnakenberg's group with main interest in microelectrodes on flexible substrates for biological and biomedical applications.

Aaron Babendreyer received his M. Sci. degree with distinction in biology from RWTH Aachen University in 2012. He started a research project in the field of mechanobiology at the University Hospital RWTH Aachenand at the Institute of Pharmacology and ToXicology at RWTH Aachen University in the group of Prof. Ludwig. In 2018, he received his Dr. rer. nat. degree with distinction from the RWTH Aachen University. Since 2012, he is head of the research group "Vascular Mechanobiology and Inflammation" at the Institute of Molecular Pharmacology at University Hospital RWTH Aachen.

Christina Hoffmann completed an apprenticeship as a biology laboratory technician at the Forschungszentrum Jülich between 2011 and 2014. From 2014 to 2017, she studied Biological Sciences at the Zuyd Hogeschool in Heerlen, The Netherlands, and received her Bachelor degree in 2017. Since then she is working as laboratory assistant at the Forschungszentrum Jülich.

Sven Gerlach completed an apprenticeship as a biology laboratory technician at the Forschungszentrum Jülich between 2016 and 2019 and has been working there since then. Since 2019, he is additionally studying Biomedical Science at the Faculty of Science and Technology at Zuyd University in Heerlen, The Netherlands.

Tom Kremers received his master's degree in electrical engineering from RWTH Aachen University Aachen in 2015. Until July 2020, he was a PhD student at the Institute of Materials in Electrical Engineering 1 at RWTH Aachen University in Prof. Schnakenberg's group. His main research is on development of digital microfluidic systems with embedded electrochemical sensors.

Andreas Ludwig studied biology at the University of Kiel, Germany. He is the director of the Institute of Molecular Pharmacology at the RWTH Aachen University. A major focus of his research is on the regulation and activity of ADAM-family metalloproteinase in inflammatory diseases. A recent research project investigates how mechanical forces modulate the inflammatory response of endothelial cells.

Bernd Hoffmann studied biology at the Technical University Hannover, Germany, and received his diploma in 1995. For his Ph.D., he went to Erlangen and Go¨ttingen and received his doctorate degree (rer. nat.) in 2000. From 2000 to 2002, he went to the University of Medicine and Dentistry of New Jersey (USA) as postdoc. In 2002, he turned back to Germany to work as group leader at the Forschungszentrum Jülich since then. From 2004 to 2015, he additionally worked as associated lecturer at the University of Bonn, Germany, where he also received his habilitation in 2015 to become member of the Faculty of Mathematics and Natural Sciences.

Rudolf Merkel studied general physics at the Technical University Munich, Germany, and received his Dipl.-Phys degree in 1988. After he received his Ph.D. from the same university in 1993, he went to the University of British Columbia (Vancouver, BC, Canada) were he stayed as postdoc for two years. Subsequently, he returned to Munich as leader of an independent junior research group. He was appointed as director of an institute at the Forschungszentrum Jülich in 2001 and one year later as full professor in Physical Chemistry at Bonn University, Germany.

Stefan Uhlig studied biochemistry at Tübingen University, Germany. After stations at Konstanz University, Germany, and the Research Center Borstel, Germany, he became the chair of Institute of Pharmacology and ToXicology at RWTH Aachen University in 2006. Since 2011, he is dean of the Medical Faculty of RWH Aachen University.

Uwe Schnakenberg studied physics at University Bonn and at RWTH Aachen University. He worked 10 years with Fraunhofer Institute for Silicon Technology in Berlin, Germany, on innovative microsystem technologies and microsystems. He turned back to RWTH Aachen University working as research director at the Institute for Materials in Electrical Engineering 1 (IWE 1) responsible for the development of microsystems for life science applications. In 2003, he received the EUROSENSORS XVII Fellow Award for his contributions in sensor technologies. In 2015, he was appointed as adjunct professor. Today, his interest is on the development of microfluidic systems.